INTERNATIONAL JOURNAL FOR NUMERICAL METHODS IN FLUIDS
Int. J. Numer. Meth. Fluids 2003; **42**:117–130 (DOI: 10.1002/fld.447)

Annular liquid jets at high Reynolds numbers

G. Georgiou*,†

Department of Mathematics and Statistics, University of Cyprus, P.O. Box 20537, 1678 Nicosia, Cyprus

SUMMARY

The flow of annular liquid jets at high Reynolds numbers is analysed by means of the finite element method and the full-Newton iteration scheme. Results have been obtained for various values of the inner to the outer diameter ratio and for non-zero surface tension, using extremely long meshes. The annular film moves far from the symmetry axis at low values of the Reynolds number. At higher Reynolds numbers, the film moves towards the axis of symmetry and appears close to very far downstream, forming a round jet. Asymptotic results for the radius of the resulting round jet are provided. Copyright © 2003 John Wiley & Sons, Ltd.

KEY WORDS: annular jet; extrusion; finite elements; Reynolds number; surface tension

1. INTRODUCTION

Laminar annular liquid jets have been the subject of many studies in the past few decades, since they appear in many polymer processing applications, such as the annular extrusion for the manufacturing of pipes, the film blowing, the blow molding and the wire coating processes [1, 2], as well as in chemical reactors, such as inertial confinement fusion reactors [3, 4]. Analyses accounting for both surface tension and gravity effects at non-zero Reynolds numbers appeared very recently [5, 6].

Ramos [5] studied annular liquid jets at high Reynolds numbers and analysed them asymptotically for large and small capillary numbers, using a perturbation method based on a long wavelength approximation. Housiadas *et al.* [6], numerically solved the steady Newtonian annular extrusion flow, and studied the effects of gravity and surface tension forces on the shape of the extrudate, under the assumption that the closing length is large, i.e. the jet closes far downstream from the exit plane of the computational domain. In their numerical simulations, they used the finite element method with the Newton–Raphson iterative scheme for the calculation of the unknown positions of the inner and outer free surfaces, i.e. the positions of the two surfaces are calculated simultaneously with the other unknown fields [6, 7]. Further references concerning annular extrusion and annular liquid jets are provided in

*Correspondence to: G. Georgiou, Department of Mathematics and Statistics, University of Cyprus, P.O. Box 20537, 1678 Nicosia, Cyprus.
†E-mail: georgios@ucy.ac.cy

Received June 2001
Revised 15 July 2002

References [5, 6, 8]. References concerning extrusion simulations in general can be found in Reference [9].

The objective of the present work is to investigate, by means of numerical simulations, the flow of annular liquid jets at high Reynolds numbers for various values of the inner to outer diameter ratio and non-zero surface tension. The governing equations and the boundary conditions of the flow are presented in Section 2, while the finite element formulation is presented in Section 3. The numerical results are presented and discussed in Section 4. At high Reynolds numbers, the film moves towards the axis of symmetry and appears to close very far downstream, forming a round jet. Asymptotic results for the radius of the resulting round jet are provided in Section 5. Our conclusions are summarized in Section 6.

2. GOVERNING EQUATIONS

The geometry of the annular extrusion process is illustrated in Figure 1. Under the influence of inertia and surface tension, the annular film closes at a distance from the die exit known as the *closing* [10] or *convergence length* [4]. The exit plane of the computational domain is taken upstream from the closing point, as shown in Figure 2. The flow is assumed to be steady, incompressible, isothermal, and Newtonian, and gravity is neglected. The governing equations are non-dimensionalized by scaling lengths by the annulus gap size $(R_2 - R_1)$, where R_1 and R_2 are the inner and outer radii of the annulus, respectively; the velocity vector, $\mathbf{v}$, is scaled by the average velocity U in the annulus, and the pressure, p, and the stress tensor, τ, by $\mu U/(R_2 - R_1)$, where μ is the constant viscosity. The resulting dimensionless forms of the continuity and momentum equations are

$$\nabla \cdot \mathbf{v} = 0 \tag{1}$$

$$Re\ \mathbf{v} \cdot \nabla \mathbf{v} = -\nabla p - \nabla \cdot \tau \tag{2}$$

where

$$Re \equiv \frac{\rho U (R_2 - R_1)}{\mu} \tag{3}$$

is the Reynolds number, and ρ is the density.

The boundary conditions of the flow are shown in Figure 2. The kinematic condition on the two free surfaces,

$$\mathbf{n} \cdot \mathbf{v} = 0 \tag{4}$$

where $\mathbf{n}$ is the unit normal vector pointing outwards from a free surface, requires that these remain material surfaces. From the momentum balance on any free surface, we get

$$\mathbf{n} \cdot \mathbf{T} = -\frac{2H}{\mathrm{Ca}} \mathbf{n} \tag{5}$$

where

$$\mathbf{T} = -p\mathbf{I} - \tau = -p\mathbf{I} + \nabla \mathbf{v} + (\nabla \mathbf{v})^{\mathrm{T}} \tag{6}$$

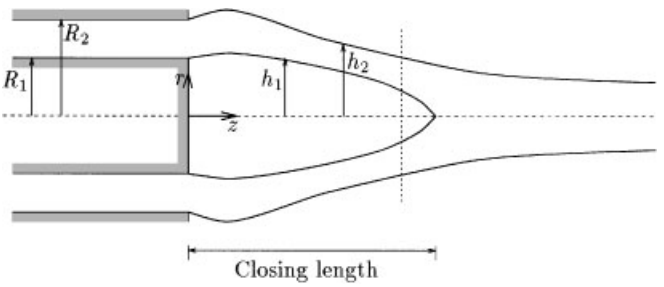

Figure 1. Schematic of the annular extrusion flow. The vertical dotted line indicates the exit plane of the computational domain.

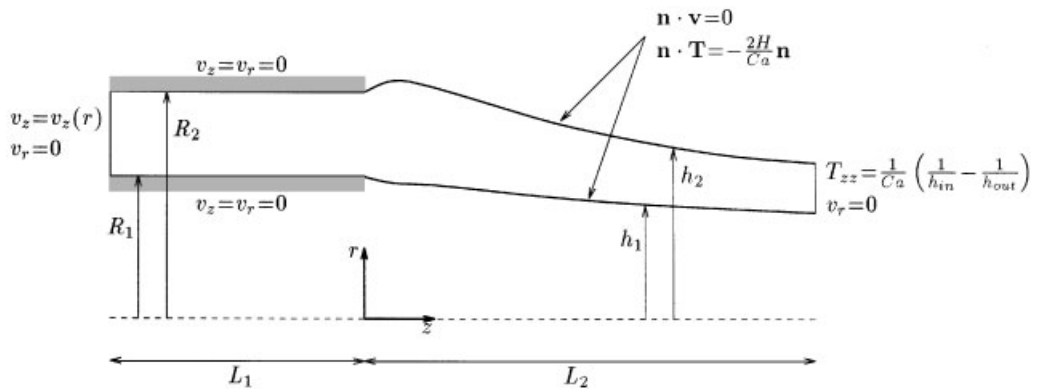

Figure 2. Geometry and boundary conditions of the annular extrusion flow.

is the total stress tensor, and $\mathbf{I}$ is the unit tensor; Ca is the capillary number, defined by

$$\mathrm{Ca} \equiv \frac{\mu U}{\sigma} \tag{7}$$

where σ denotes the surface tension, and $2H$ is the mean curvature of a free surface, given by

$$-2H = \frac{h_{zz}}{[1+h_z^2]^{3/2}} - \frac{1}{h\sqrt{1+h_z^2}} \tag{8}$$

Note that the subscripts z and zz denote first- and second-order differentiation of h with respect to z.

Along the solid walls, both the velocity components vanish. At the inlet plane, taken at a distance L_1 upstream the die exit, the flow is assumed to be fully developed, i.e. v_r is zero and v_z is given by the standard solution for Poiseuille flow in an annulus. Finally, at the outlet plane, taken at a distance L_2 downstream from the die exit, the flow is assumed to be approximately uniform, and thus,

$$T_{zz} = -p - \tau_{zz} = \frac{1}{\mathrm{Ca}}\left(\frac{1}{h_2} - \frac{1}{h_1}\right) \quad \text{and} \quad v_r = 0 \tag{9}$$

where τ_{zz} is the normal stress component. (Note that the subscript zz denotes here the zz stress component.) The above outflow boundary conditions have been shown to lead to satisfactory results up to a certain fraction of the length L_2, provided that the latter is sufficiently large [6].

3. FINITE ELEMENT FORMULATION

The annular extrusion flow problem has been solved using finite elements. The unknown positions of the inner and outer free surfaces, respectively, are calculated simultaneously with the pressure and velocity fields, using the Newton method (i.e., without the use of Picard iterations). The flow domain is discretized by means of curvilinear (biquadratic), quadrilateral isoparametric elements. The pressure, p, and the velocity, $\mathbf{v}$, are approximated by means of bilinear, Ψ^j, and biquadratic, Φ^j, basis functions

$$\bar{p}=\sum_{j=1}^{N_p} p_j\Psi^j \quad \text{and} \quad \bar{\mathbf{v}}=\sum_{j=1}^{N_\mathbf{v}} \mathbf{v}_j\Phi^j \tag{10}$$

where bars denote the approximations of the unknown fields, N_p and $N_\mathbf{v}$ are the numbers of pressure and velocity notes, respectively, and p_j and $\mathbf{v}_j$ denote the values of $\bar{p}$ and $\bar{\mathbf{v}}$ at the jth node. The standard Galerkin method is used, i.e. the continuity the momentum equations are weighted over the flow domain Ω with the bilinear and biquadratic basis functions, respectively, and the divergence theorem is applied to the total stress term of the momentum equation. Thus, the discretized continuity and momentum equations are as follows:

$$\int_\Omega \nabla\cdot\bar{\mathbf{v}}\Psi^i\,\mathrm{d}V=0, \quad i=1,\ldots,N_p \tag{11}$$

$$\int_\Omega [Re\bar{\mathbf{v}}\cdot\nabla\bar{\mathbf{v}}\Phi^i+\bar{\mathbf{T}}\cdot\nabla\Phi^i]\,\mathrm{d}V-\int_{\partial\Omega}\mathbf{n}\cdot\bar{\mathbf{T}}\,\mathrm{d}S=\mathbf{0}, \quad i=1,\ldots,N_\mathbf{v} \tag{12}$$

where $\mathbf{n}$ is the outward unit normal to the boundary $\partial\Omega$. The unknown positions, h_1 and h_2, of the free surfaces of the annular extrudate are expanded in terms of quadratic basis functions, $\mathscr{X}^j$, conforming to the isoparametric transformation:

$$\bar{h}_1=\sum_{j=1}^{N_h} h_{1j}\mathscr{X}^j \quad \text{and} \quad \bar{h}_2=\sum_{j=1}^{N_h} h_{2j}\mathscr{X}^j \tag{13}$$

where N_h is the number of free surface nodes, and h_{1j} and h_{2j} the nodal values of $\bar{h}_1$ and $\bar{h}_2$, respectively. The functions $\mathscr{X}^j$ are also used to weight the kinematic condition on the two free surfaces, denoted here by $\partial\Omega_1$ and $\partial\Omega_2$:

$$\int_{\partial\Omega_1}\mathbf{n}\cdot\bar{\mathbf{v}}\mathscr{X}^i\,\mathrm{d}S=0, \quad i=1,\ldots,N_h \tag{14}$$

and

$$\int_{\partial\Omega_2}\mathbf{n}\cdot\bar{\mathbf{v}}\mathscr{X}^i\,\mathrm{d}S=0, \quad i=1,\ldots,N_h \tag{15}$$

The boundary conditions on the two free surfaces and the outflow plane are imposed by substituting the stress components, as given by Equations (5) and (9), respectively, in the boundary integral of Equation (12). Equations (11), (12), (14) and (15) constitute a non-linear system of $N_p + 2N_v + 2N_h$ equations, which is solved using the Newton method and a standard frontal subroutine. In the extrudate region, the r-co-ordinates of the mesh nodes are updated at each iteration, according to the newly found positions of the inner and outer free surfaces. For this purpose, the spine technique is employed, i.e. the nodes move in the radial direction so that the ratios of the widths of the elements to the thickness of the annular film remain constant.

4. NUMERICAL RESULTS AND DISCUSSION

We used meshes of different lengths and degrees of refinement, in order to confirm the validity of the numerical results. All meshes were graded, with the element dimensions becoming progressively smaller towards the exit and the walls of the annulus. In this section, we present calculations obtained with the two longest meshes corresponding to $L_1 = 50$, and $L_2 = 6400$ and 20 000, respectively. Useful data for these two meshes are provided in Table 1; N_z and N_r denote the numbers of elements in the axial and radial directions, respectively.

Results have been obtained for three different values of the ratio

$$\kappa \equiv \frac{R_1}{R_2} \tag{16}$$

of the inner to the outer diameter of the annulus: 0.5, 10/11, and 20/21. We first studied the case in which surface tension is zero (i.e., $\mathrm{Ca} = \infty$). In Figure 3, we show the calculated film profiles for $\kappa = 0.5$ and various Reynolds numbers. We observe that the film moves slightly away from the axis of symmetry at small values of the Reynolds number. However, as the Reynolds number is increased, the film starts moving towards the symmetry axis. This behaviour agrees with experimental observations [11]. In Figure 4, we compare the final values of the internal and external radii of the annular film obtained with Mesh 1 ($L_2 = 6400$) and Mesh 2 ($L_2 = 20000$). Small differences appear for Reynolds numbers above 1000, with the prediction of the shorter mesh being slightly above that of the longer one.

The effect of the Reynolds number on the shape of the annular film is more pronounced when κ is higher. This is illustrated in Figures 5 and 6, where we show results for $\kappa = 10/11$ and 20/21, respectively. The comparison of the final values of the internal and external film radii calculated with the two meshes reveals that the calculations are converged only for moderate Reynolds numbers: up to $Re = 30$ for $\kappa = 10/11$ and up to $Re = 20$ for $\kappa = 20/21$. It is worthy to note here that these values of the Reynolds number would have been much higher, if a different length scale were used, i.e., R_1 instead of $(R_2 - R_1)$. (In such a case,

Table 1. Data for two of the meshes used in the present work.

Mesh	L_2	N_z	N_r	Number of elements	Number of unknowns
1	6400	373	10	3730	36855
2	20000	455	16	7280	69481

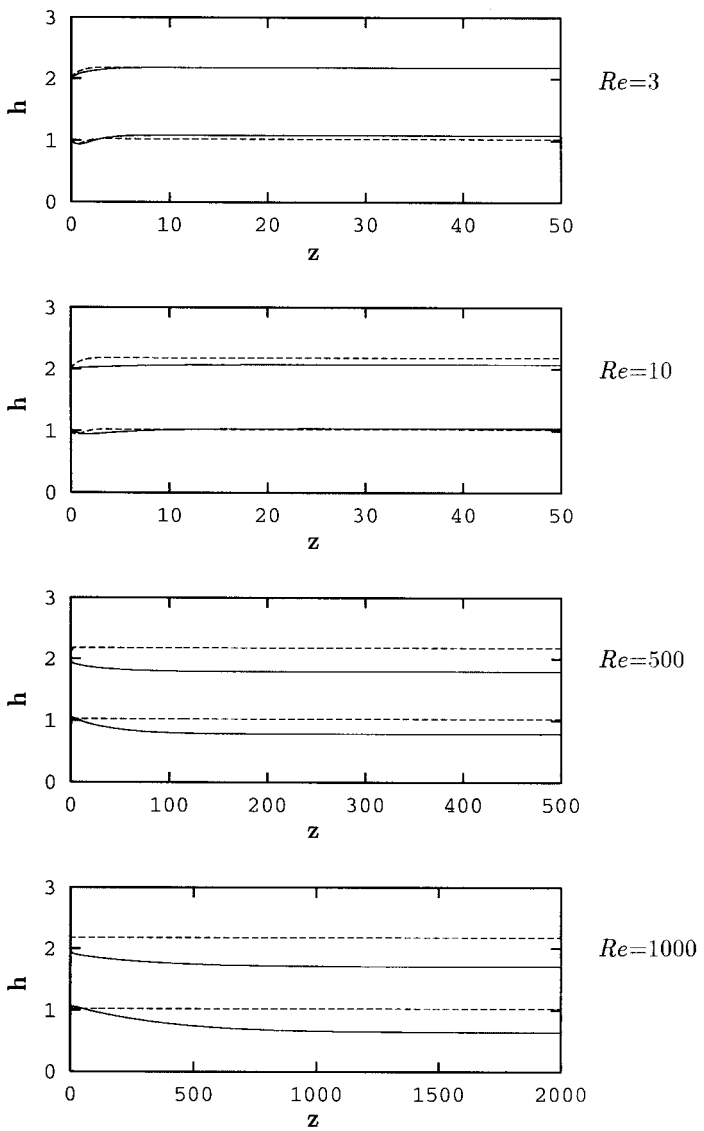

Figure 3. Annular film shapes for various Reynolds numbers, $\kappa = 0.5$ and zero surface tension, obtained with $L_2 = 20\,000$. The broken lines show the annular film at zero Reynolds number.

Re must be multiplied by 10 and 20 for $\kappa = 10/11$ and $20/21$, respectively.) Another remark is that the numerical solutions obtained with the shorter mesh at high Reynolds numbers do not differ practically from those obtained with the longer mesh up to a distance downstream from the exit of the die which is roughly equal to 2000 (see Figure 7).

The outwards motion of the film at low Reynolds numbers is much more appreciable for higher values of κ, i.e., for $\kappa = 20/21$ (Figure 6). A consequence of this motion is the reduction of the film thickness, due to mass conservation. This reduction is counterbalanced by the film

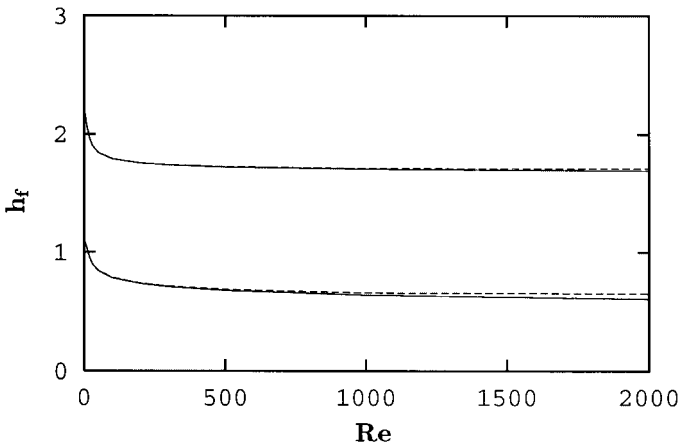

Figure 4. Final value of the internal and external radii of the annular film with $L_2 = 6400$ (broken line) and 20 000 (solid line); $\kappa = 0.5$, zero surface tension.

swelling when κ is small (see, e.g., Figure 3), and is more dramatic for higher values of κ. Evidently, for even higher values of κ the reduction of the thickness will result in the break up of the film, which means that such a flow is not realizable in practice. However, the break up of the film may be delayed up to higher diameter ratios in case of non-zero surface tension, since the latter pushes the film towards the symmetry axis, or in the presence of gravity (acting in the direction of the flow) [6].

The contractive action of the surface tension is illustrated in Figure 8, where annular film shapes obtained for $\kappa = 10/11$, $Re = 10$ and 30, and various capillary numbers are plotted. We observe that surface tension reduces the closing length of the annular film considerably. As illustrated in Figure 9 where we zoom near the exit of the die, initially, the shape of the annular film is almost independent of the capillary number, since the three shapes in Figures 8a and b coincide. This result agrees with the asymptotic solutions provided by Ramos [5]. Similar observations have been made for different values of the diameter ratio κ and other values of the Reynolds number.

5. ASYMPTOTIC RESULTS FOR THE OUTER JET DIAMETER

The theoretical limits of the outer jet diameter at infinite Reynolds number $h_{2,\infty}$, are obtained by taking mass and momentum balances between the exit of the die, where the flow is assumed to be fully developed, and at a plane very far downstream in the film region, where the flow is taken as plug. With such an analysis, the asymptotic limits of the extrudate-swell ratio at infinite Reynolds number are predicted for the round and planar Newtonian jets. In the former case this limit is $\sqrt{3}/2$ [12], whereas in the latter is $\frac{5}{6}$ [13].

By using the dimensionless form of the continuity equation, one obtains

$$u_{z,\infty}(h_{2,\infty}^2 - h_{1,\infty}^2) = 1 - \kappa^2 \tag{17}$$

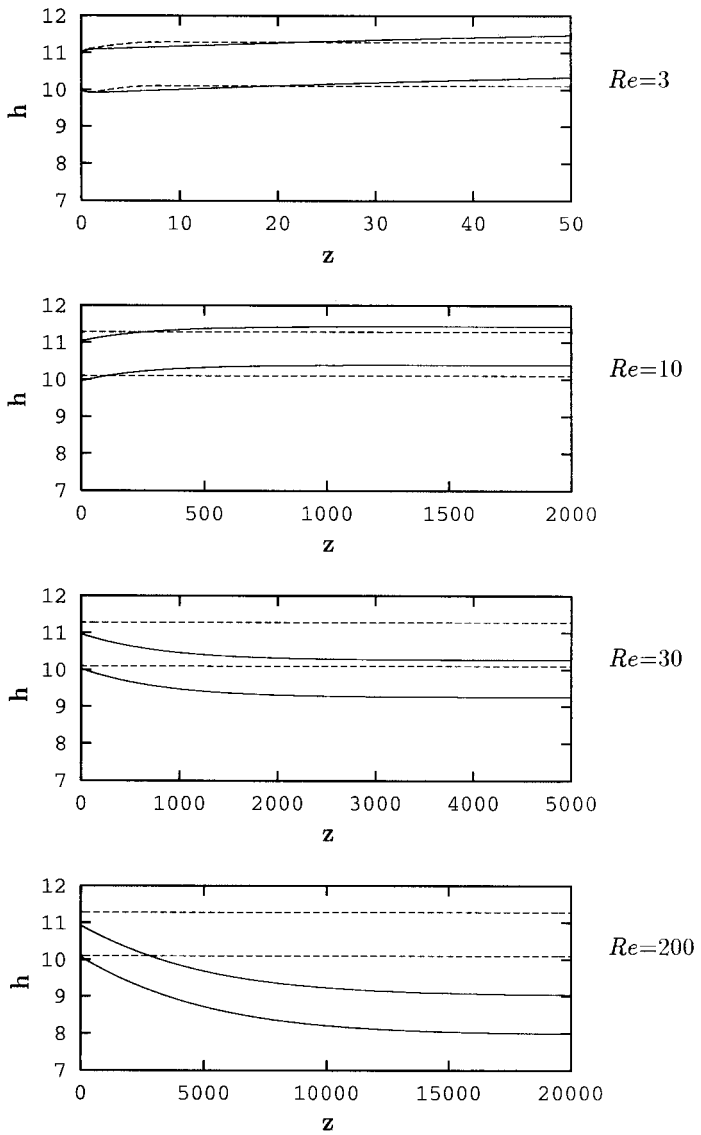

Figure 5. Annular film shapes for various Reynolds numbers, $\kappa = 10/11$ and zero surface tension, obtained with $L_2 = 20\,000$. The broken lines show the annular film at zero Reynolds number.

where the subscript ∞ denotes the outflow quantities at the asymptotic limit, and κ is the ratio of the inner to the outer die radius. (The dimensionless outer radius is equal to unity.) From the conservation of momentum, we may write

$$u_{z,\infty}^2(h_{2,\infty}^2 - h_{1,\infty}^2) = 2\int_{\kappa}^{1} u_z^2 r \, \mathrm{d}r \tag{18}$$

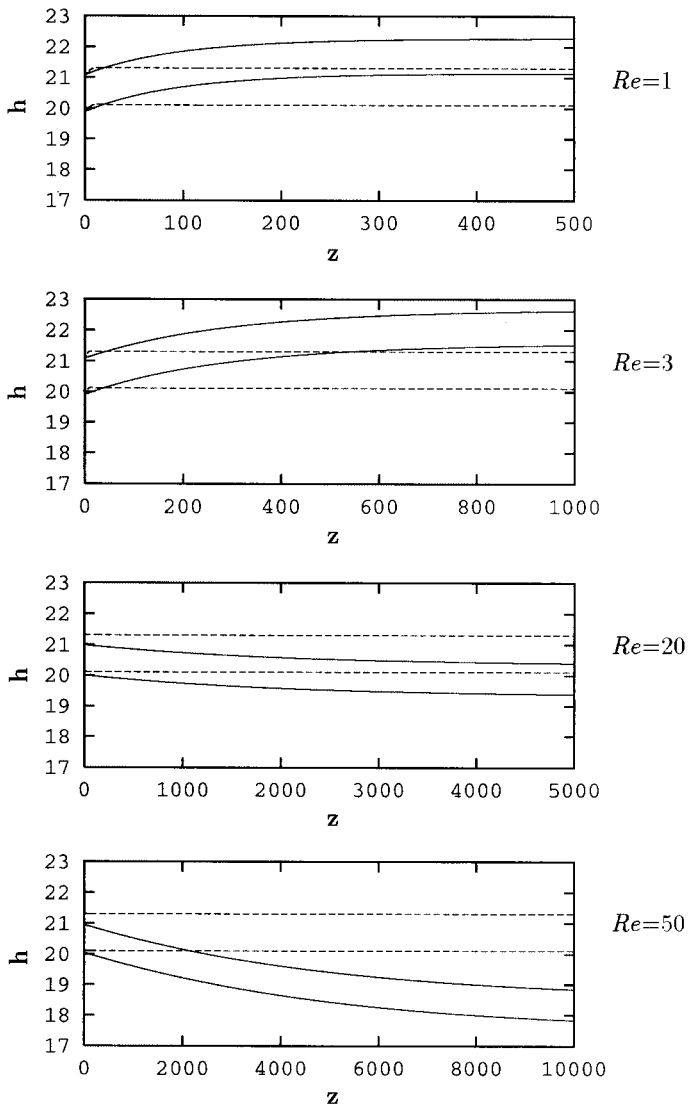

Figure 6. Annular film shapes for various Reynolds numbers, $\kappa = 20/21$ and zero surface tension, obtained with $L_2 = 20\,000$. The broken lines show the annular film at zero Reynolds number.

where the velocity u_z is given by [14]

$$u_z = 2\left(1 - r^2 - \frac{1-\kappa^2}{\ln \kappa}\ln r\right)\Big/\left(1 + \kappa^2 + \frac{1-\kappa^2}{\ln \kappa}\right) \tag{19}$$

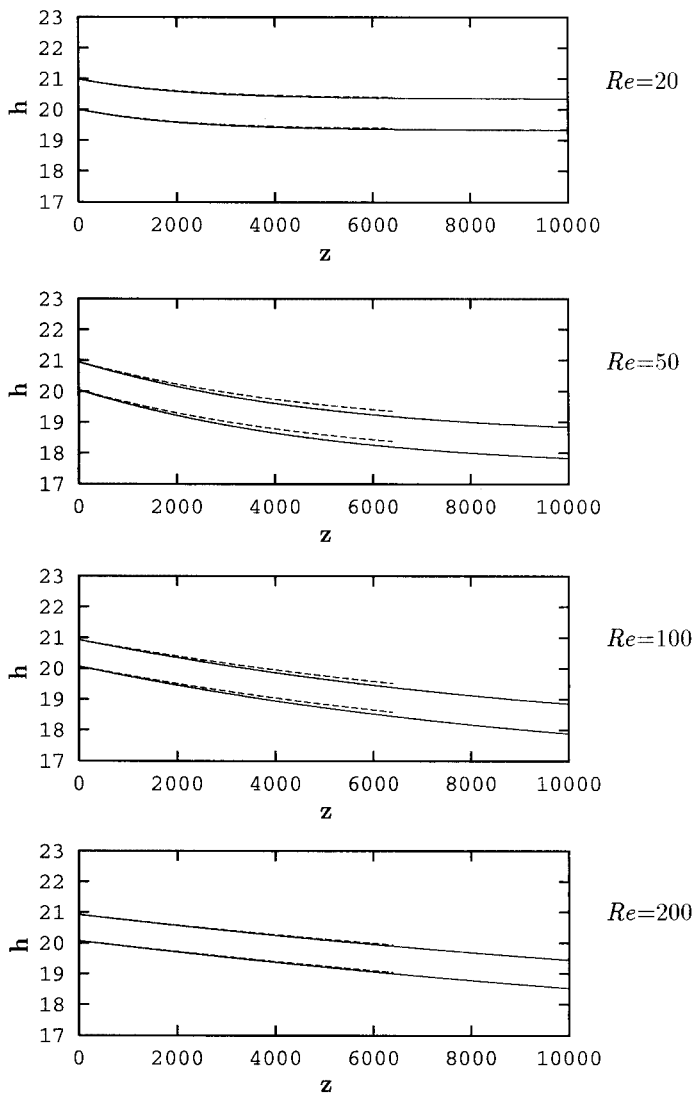

Figure 7. Shapes of the annular film with $L_2 = 6400$ (broken line) and 20 000 (solid line); $\kappa = 20/21$, zero surface tension.

Combining Equations (11) and (12) gives

$$h_{2,\infty}^2 - h_{1,\infty}^2 = \frac{(1-\kappa^2)^2}{2\int_\kappa^1 u_z^2 r \, \mathrm{d}r} \tag{20}$$

By substituting Equation (13) into Equation (14) and by integrating, we find that

$$h_{2,\infty}^2 - h_{1,\infty}^2 = F(\kappa) \tag{21}$$

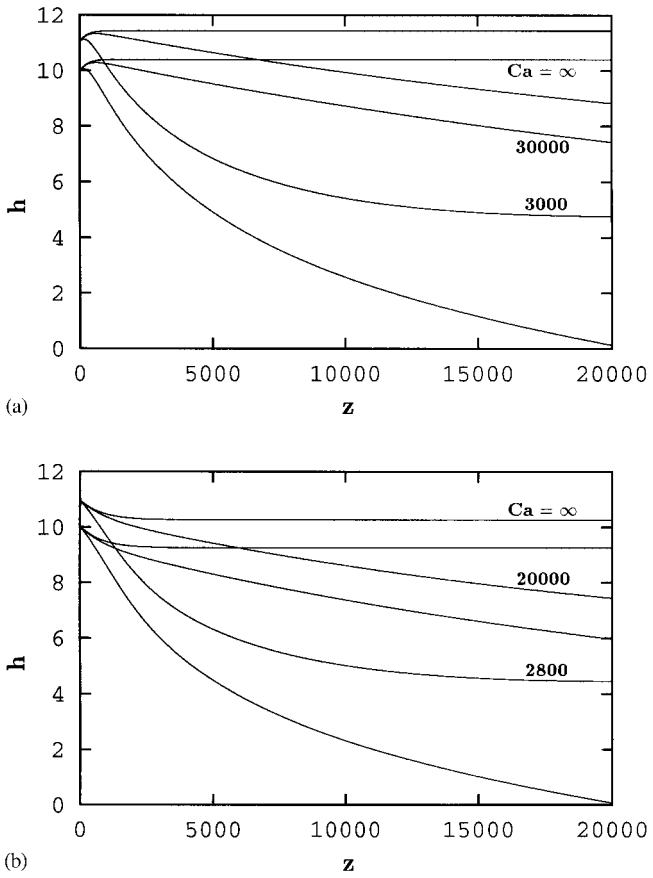

Figure 8. Surface tension effect for: (a) $Re=10$; and (b) $Re=30$; $\kappa=10/11$.

where

$$F(\kappa)\equiv\frac{3(1-\kappa^2)[(1+\kappa^2)\ln\kappa+(1-\kappa^2)]^2}{4(1+\kappa^2+\kappa^4)\ln^2\kappa+9(1-\kappa^4)\ln\kappa+6(1-\kappa^2)^2} \tag{22}$$

Due to the presence of two unknowns, $h_{1,\infty}$ and $h_{2,\infty}$, the above analysis does not provide any information as to whether the two free surfaces level off without closing or the jet closes far downstream, as indicated by the numerical calculations. However, if we assume that the jet closes far downstream, i.e., $h_{1,\infty}$ is zero, then the radius of the resulting round jet is $h_{2,\infty}=\sqrt{F(\kappa)}$. In Figure 10a, $\sqrt{F(\kappa)}$ is plotted versus κ. In Figure 10b, we plot the same quantity scaled by the gap size $(1-\kappa)$. Note that as $\kappa\to 0$, $\sqrt{F(\kappa)}/(1-\kappa)$ tends to $\sqrt{3}/2$, which is the asymptotic ratio for the round jet. Of course, in this case $h_{1,\infty}$ is zero. As for the other limiting case of $\kappa\to 1$, one may expect the very thin annular jet to behave as a planar jet remaining horizontal and reaching the corresponding asymptotic ratio

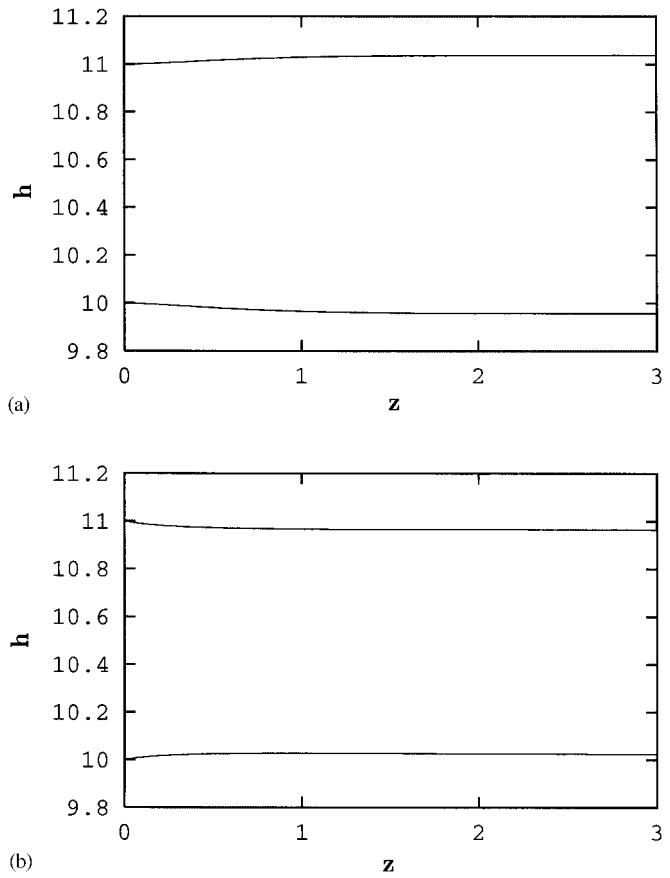

Figure 9. Surface tension effect is not important near the exit: (a) $Re = 10$ and $\mathrm{Ca} = \infty, 30\,000$ and 3000; and (b) $Re = 30$ and $\mathrm{Ca} = \infty$, 20 000 and 2800; $\kappa = 10/11$.

of $\frac{5}{6}$. Our calculations showed that the jet exhibits such a behaviour initially but closes to a round jet infinitely far downstream, the asymptotic radius of which is equal to $\sqrt{F(\kappa)}$. Despite the fact that this value appears to vanish as $\kappa \to 1$, it is many times bigger than the annular gap size $(1 - \kappa)$, as illustrated in Figure 10. This limiting case is only of theoretical interest, since the thin annular film is physically expected to break up at high Reynolds numbers.

6. CONCLUSIONS

We have used finite elements to solve the steady flow of an annular Newtonian jet at high Reynolds numbers, and obtained results for various values of the inner to the outer diameter ratio and non-zero surface tension. The numerical simulations have shown that at low values of the Reynolds number, the annular film moves far from the symmetry axis, whereas, at

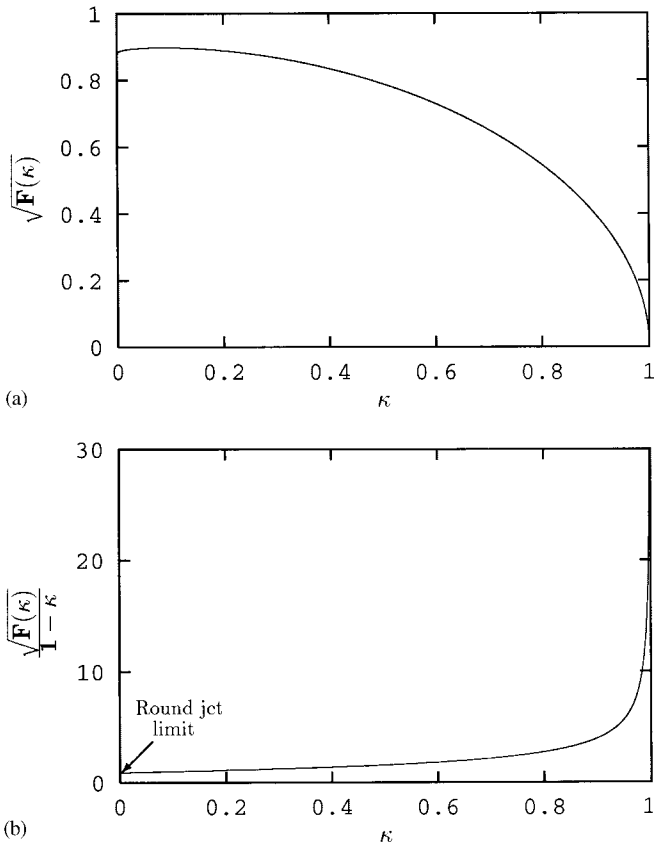

Figure 10. The behaviour of the function $F(\kappa)$.

higher Reynolds numbers, the film moves towards the axis of symmetry and appears to close very far downstream, forming a round jet. The radius of the latter, which is a function of the diameter ratio, has been calculated in the limit of infinite Reynolds number, using an asymptotic analysis.

REFERENCES

1. Housiadas K, Tsamopoulos J. Unsteady extrusion of a viscoelastic film: I. General model and its numerical solution. *Journal of the Non-Newtonian Fluid Mechanics* 2000; **88**:229–259.
2. Housiadas K, Tsamopoulos J. Unsteady extrusion of a viscoelastic film: II. Linearized model and its analytical solution. *Journal of the Non-Newtonian Fluid Mechanics* 2000; **88**:303–325.
3. Esser PD, Abdel-Khalik SI. Dynamics of vertical annular liquid jets. *ASME Journal of Fluids Engineering* 1984; **106**:45–51.
4. Kihm KD, Chigier NA. Experimental investigations of annular liquid curtains. *ASME Journal of Fluids Engineering* 1990; **112**:61–66.
5. Ramos JI. Annular liquid jets and other axisymmetric free-surface flows at high Reynolds numbers. *Applied Mathematical Modelling* 1998; **22**:423–452.
6. Housiadas K, Georgiou G, Tsamopoulos J. The steady annular extrusion of a Newtonian liquid under gravity and surface tension. *International Journal for Numerical Methods in Fluids* 2000; **33**:1099–1119.

7. Georgiou GC, Papanastasiou TC, Wilkes JO. Laminar jets at high Reynolds and high surface tension. *AIChE Journal* 1988; **24**:1559–1562.
8. Huynh BP. A numerical investigation of non-isothermal extrusion through annular dies. *International Journal of Engineering and Science* 1998; **36**:171–188.
9. Georgiou GC, Boudouvis A. Converged solutions of the Newtonian extrudate swell problem. *International Journal for Numerical Methods in Fluids* 1999; **29**:363–371.
10. Hassan MZ, Mitsutake Y, Monde M. Shape of an annular liquid jet. *ASME Journal of Fluids Engineering* 1997; **119**:591–596.
11. Baird MHI, Davidson JF. Annular jets—I Fluid Dynamics. *Chemical Engineering Science* 1962; **17**:467–472.
12. Harmon DB. Drop sizes from low speed jets. *Journal of the Franklin Institute* 1955; **259**:519–522.
13. Tillet JPK. On the laminar flow in a free jet of liquid at high Reynolds numbers. *Journal of Fluid Mechanics* 1968; **32**:273–292.
14. Papanastasiou T, Georgiou G, Alexandrou A. *Viscous Fluid Flow*. CRC Press: Boca Raton, FL, 1999.

